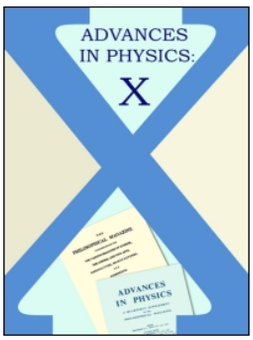

Advances in Physics: X

ISSN: (Print) 2374-6149 (Online) Journal homepage: https://www.tandfonline.com/loi/tapx20

Heteroaggregation of ceramic colloids in suspensions

M. Cerbelaud, A. Videcoq, F. Rossignol, M.A. Piechowiak, D. Bochicchio & R. Ferrando

To cite this article: M. Cerbelaud, A. Videcoq, F. Rossignol, M.A. Piechowiak, D. Bochicchio & R. Ferrando (2017) Heteroaggregation of ceramic colloids in suspensions, Advances in Physics: X, 2:1, 35-53, DOI: 10.1080/23746149.2016.1254064

To link to this article: https://doi.org/10.1080/23746149.2016.1254064

Published online: 13 Nov 2016.

ADVANCES IN PHYSICS: X, 2017
VOL. 2, NO. 1, 35–53
http://dx.doi.org/10.1080/23746149.2016.1254064

Taylor & Francis
Taylor & Francis Group

REVIEW ARTICLE

OPEN ACCESS

Heteroaggregation of ceramic colloids in suspensions

M. Cerbelaud[a], A. Videcoq[a], F. Rossignol[a], M.A. Piechowiak[a], D. Bochicchio[b] and R. Ferrando[c,d]

[a]University of Limoges, CNRS, ENSCI, SPCTS, UMR 7315, Limoges, France; [b]Physics Department of the University of Genoa, Genoa, Italy; [c]Chemistry and Industrial Chemistry Department, University of Genoa, Genoa, Italy; [d]IMEM/CNR, Genoa, Italy

ABSTRACT

The colloidal route is an important methodology in ceramic processing. A key step of the colloidal route is the aggregation of colloids in suspension. This often involves colloids of different types, in a process which is known as heteroaggregation. Here we review the recent developments in ceramic heteroaggregation, focusing on the physical mechanisms that cause it and on the structural properties of the resulting aggregates. Structural properties are analysed both on the local scale, at the level of nearest-neighbour contacts between colloids and on the long-range scale, at which percolating aggregates form, leading to gelification. Both experimental and simulation results are reviewed. The effects of the structure of the aggregates on the subsequent steps of ceramic processing are discussed.

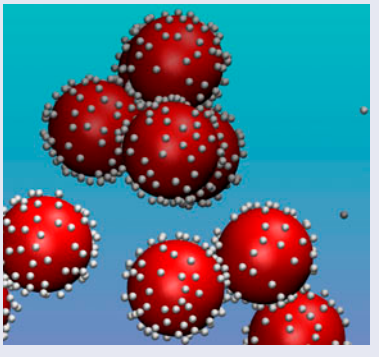

ARTICLE HISTORY
Received 16 December 2015
Accepted 21 October 2016

KEYWORDS
Ceramics; suspensions; aggregation; Brownian simulations

PACS
82.70.Dd colloids; 82.70.Gg gels and sols; 82.70.Kj emulsions and suspensions; 83.80.Hj suspensions; dispersions; pastes; slurries; colloids

1. Introduction

In recent years, there has been a growing interest in new methods for ceramic materials processing. An important step forward in this field has been the development of colloidal processing [1]. Colloidal processing is suitable for reliably producing ceramic films and bulk materials. This type of processing requires

CONTACT R. Ferrando ferrando@fisica.unige.it

the control of the initial suspension structure and of its subsequent evolution through different fabrication stages, which can be schematically summarized as follows (see Figure 1): (1) powder synthesis, (2) suspension preparation, (3) consolidation into the desired component shape, (4) removal of the solvent phase and (5) densification to produce the desired final microstructure, for example with the desired spatial distribution of phases and with controlled porosity.

All steps in this process require careful attention. Specifically, heterogeneities and defects introduced in the first steps may persist or even worsen during the final densification stage [1]. Therefore, there is a growing interest towards understanding the phenomena that occur during aggregation in suspension, possibly elucidating the elementary physical mechanisms. With this respect, the interplay of experiments and computer simulations is of great importance, since simulations are extremely useful in following the elementary steps of the aggregation process.

Heteroaggregation of colloids has received more and more interest since few years [2–4]. Particular attention has been paid for example on the determination of the absolute heteroaggregation rate constants [5]. Moreover heteroaggregation is also more and more studied as a step in the synthesis of a variety of materials (see for example [6–13]), including ceramic materials [14–34].

In heteroaggregation, two types of colloids are dispersed in a suspension. If these colloids acquire opposite charges, this may induce aggregation driven by electrostatic interactions, with subsequent flocculation and precipitation. The heteroaggregation process is quite complex, and depends on a series of parameters, such as solute volume fraction, suspension composition, pH, size ratio between the two types of colloids etc.

In this Review, we focus on the recent results that have shed light on the heteroaggregation mechanisms of ceramic colloids. In Section 2 we summarize the basic points about the interactions between charged colloids in a suspension,

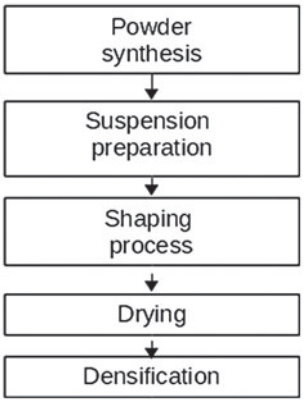

Figure 1. Main stages of colloidal processing for ceramics.

with the aim of underlining the differences between suspensions of unary and binary colloids. In Section 3, we review the recent experimental and simulation results on ceramic heteroaggregation. That Section is divided into two parts. In Sections 3.2 and 3.1 we consider heterocolloids with large size small size differences, respectively. The focus of these Sections is on relating aggregation mechanisms and resulting aggregate shapes, both on the local scale (nearest-neighbour contacts) and on the long-range scale (percolating aggregates leading to gelification). Section 4 contains the conclusions.

2. Colloid–colloid interactions in suspension: unary vs. binary colloids

Let us consider the interaction between two spherical colloids i and j of radii a_i and a_j whose centres are separated by a distance r_{ij}. In the simplest model [1,35,36], this interaction consists of four terms

$$U_{ij} = U_{ij}^{\mathrm{vdW}} + U_{ij}^{\mathrm{el}} + U_{ij}^{\mathrm{steric}} + U_{ij}^{\mathrm{structural}}, \tag{1}$$

The first two terms U_{ij}^{vdW} and U_{ij}^{el} in Equation (1) correspond to van der Waals and electrostatic interactions, respectively. These terms are defined for distances $r > a_i + a_j$ and are generally dominant except when the distance r_{ij} is close to $a_i + a_j$. When the colloids come into contact, the third and the fourth terms, U_{ij}^{steric} and $U_{ij}^{\mathrm{structural}}$, may become dominant. U_{ij}^{steric} represents the interactions caused by macromolecules adsorbed on the colloid surface and $U_{ij}^{\mathrm{structural}}$ corresponds to the interactions due to the structuration of the liquid around the colloid (for example the hydration force) and possibly the interactions due to non-adsorbed species in solution (depletion interactions)[37,38].

The sum of van der Waals and electrostatic contributions constitute the well-known Derjaguin, Landau, Verwey and Overbeek (DLVO) potential [39,40], which has greatly contributed to the understanding of the behaviour of colloidal suspensions.

The van der Waals term is generally attractive for the ceramic suspensions considered in this paper. It can be obtained by integrating the $1/r_{ij}^6$ interaction due to induced dipoles over the volume of the spheres. The result is [35]:

$$U_{ij}^{\mathrm{vdW}}(r_{ij}) = -\frac{A_{ij}}{6}\left[\frac{2a_ia_j}{r_{ij}^2-(a_i+a_j)^2} + \frac{2a_ia_j}{r_{ij}^2-(a_i-a_j)^2} + \ln\left(\frac{r_{ij}^2-(a_i+a_j)^2}{r_{ij}^2-(a_i-a_j)^2}\right)\right], \tag{2}$$

where A_{ij} is the Hamaker constant for the materials of the pair ij. $U_{ij}^{\mathrm{vdW}} \to -\infty$ for surface-to-surface separation $h_{ij} = r_{ij} - a_i - a_j \to 0$.

The electrostatic interaction depends on the surface potential induced on the interacting colloidal particles by the formation of charged groups on their

surface when they are inserted in the medium. At the same time, the medium causes also a screening of the Coulomb interaction, which is thus exponentially damped and becomes of short-range type. The magnitude of these screened electrostatic interactions should be obtained from the solution of the Poisson–Boltzmann equation. Analytical solutions of the Poisson–Boltzmann equation for spherical particles are not available, so that one may either solve the equation self-consistently by numerical methods, or use approximate expressions. The second approach is the most common because it allows both large-scale computer simulations and qualitative discussions of the suspension behaviour by a limited set of parameters which have clear physical meaning.

When two colloids approach, the surface charges regulate, which can have several effects on the interparticle forces [41]. To calculate these forces, two limits are generally considered: a constant surface charge or a constant surface potential. If the charges on colloids are not fixed, but fluctuate in equilibrium with the solvent, a good approximation is to assume that the surface potential of colloids is constant. For example, oxide particles (MO) in aqueous suspensions present hydroxyl groups on their surface (M–OH). These groups have some acid–base properties and according to the pH, they can become positive ($M–OH_2^+$) or negative ($M–O^-$). Charges of oxide particles in aqueous suspensions are determined by these acid–base equilibria. Assuming a constant surface potential allows indeed to take into account the variation in the surface charges which can occur when colloids approach each other. On the other hand, for other types of colloids such as latex particles, the approximation constant surface charge may be more appropriate [42].

In the case of constant surface potential, the electrostatic interactions can be modelled by the Hogg–Healy–Fuerstenau (HHF) expression [43,44], obtained by linearizing the Poisson–Boltzmann equation:

$$U_{ij}^{\mathrm{el}}(r_{ij}) = \pi\varepsilon\frac{a_i a_j}{a_i + a_j}\left(\psi_i^2 + \psi_j^2\right)\left[\frac{2\psi_i\psi_j}{\psi_i^2 + \psi_j^2}\ln\left(\frac{1 + e^{-\kappa h_{ij}}}{1 - e^{-\kappa h_{ij}}}\right) + \ln\left(1 - e^{-2\kappa h_{ij}}\right)\right], \tag{3}$$

where ψ_i, ψ_j are the surface potentials of particles i and j, $\epsilon = \varepsilon_0\varepsilon_r$ the dielectric constant of the solvent, and κ the inverse Debye screening length, which determines the range of electrostatic interactions. The HHF expression is in principle valid when the surface potential is not too high, say up to $\psi \simeq 25\,\mathrm{mV}$. For a symmetric $z-z$ electrolyte, κ can be expressed in terms of the ionic concentration C_I, of the electron charge e, of ε and of Avogadro's number N_A

$$\kappa = \sqrt{\frac{2e^2z^2N_AC_I}{\varepsilon k_BT}}. \tag{4}$$

In practical situations, it is important to estimate the true surface potential. This is in general difficult, so that one has to resort to approximations. A common approximation is to identify the surface potential with the zeta potential (ζ). This can be justified as follows.

The electrostatic interaction potentials (for example as that in the HHF expression of Equation (3)) describe the electrostatic interactions derived from the superposition of the diffuse double layers which are around the colloids. These potentials are deduced from the Gouy–Chapman theory [37,45], which only deals with the diffuse layer (the Stern layer is not considered), implying that the ψ in Equation (3) have to be interpreted as the values of the diffuse layer potential. The potential that can be accessed experimentally is the zeta potential, which is measured in the diffuse layer on the slip plane. This is not exactly the diffuse layer potential, however it has been shown that it is a good approximation to it, especially when the ionic strength is small and when the potentials are of small magnitude [46,47].

In a unary colloidal system, all colloids acquire charges of the same sign, so that electrostatic interactions are always repulsive. Their magnitude can be used to counterbalance the effects of van der Waals attraction, in such a way that the suspension can become stable. This is schematically shown in Figure 2. At increasing electrostatic interactions (i.e. at increasing surface potential), the suspension may change its character from strongly flocculating, to weakly flocculating, and to stable.

In a suspension containing binary colloids (A and B) the situation may be quite different, since electrostatic interactions can be of different signs. The behaviour of the suspension thus depends on a complex interplay between the attractive van der Waals interactions, the repulsive A–A and B–B electrostatic interactions, and the A–B interactions, which may be either attractive or repulsive depending for example on pH.

In Figure 3(a), the zeta potential of alumina and silica in aqueous suspension is plotted as a function of pH.

For pH larger than 8.5, both colloids are negatively charged. All electrostatic interactions are repulsive and contribute to stabilizing the suspension.

In the pH range between 7 and 8, both zeta potentials are significantly large (in the range 20–30 mV) and of opposite sign, positive for alumina and negative for silica. In this case, the homogeneous alumina–alumina and silica–silica interactions are repulsive, with negligible secondary minimum, as in Figure 2(c), while heterogeneous alumina–silica interactions are attractive, even more than in Figure 2(a), because electrostatic and van der Waals contributions are both of the same sign. In this case, the forces between colloids share some resemblance with those between different ions in ionic crystals, like NaCl or CsCl, with the main qualitative difference being that electrostatic interactions in colloids are screened. However, we should expect that in these conditions, colloids will tend to aggregate. This is the regime of interest for the heteroaggregation phenomenon.

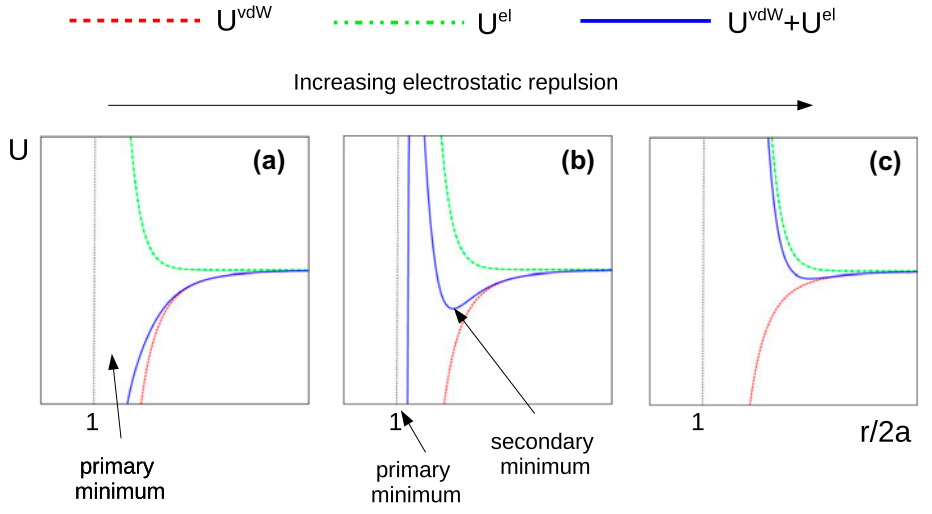

Figure 2. Schematic behaviour of the colloid–colloid interactions for unary colloids with increasing strength of the repulsive electrostatic interactions, while keeping the van der Waals contribution constant. In all panels, green dash-dotted lines correspond to the electrostatic interactions (according to Equation (3)), red dashed lines correspond to the van der Waals attraction (Equation (2)), and the blue full lines correspond to the total potential resulting from the sum of these two contributions. The vertical grey dotted line shows the distance for hard-sphere separation.
Notes: (a) For weak electrostatic interactions, the van der Waals contribution dominates, leading to aggregation in the primary minimum, whose depth is infinite if steric repulsion forces are not taken into account. (b) For a moderate increase in the electrostatic repulsion, a secondary minimum develops. Its depth is often a few k_BT, which causes mild aggregation. The primary minimum is still there, but it is separated from the secondary minimum by a larger barrier which is unlikely to be surmounted. (c) If electrostatic repulsion increases further, the secondary minimum tend to disappear, while the primary minimum remains very close to $r = 2a$ being practically unreachable. In this case, colloid aggregation is not possible and the suspension is stable. In passing from (a) to (b), the strength of the electrostatic term is doubled, whereas in passing from (b) to (c), electrostatic interactions have been increased further by a factor 10.

Opposite-sign zeta potentials are found also in the pH range between 3.5 and 7 for the binary system formed by carboxyl-functionalized silica-coated maghemite nanoparticles (cMNPs) and amino-functionalized silica nanoparticles (aSNPs), as shown in Figure 3(b) [33].

For smaller pH values, electrostatic potentials are still of different signs, but the potential on silica becomes negligible.

In the absence of organic additives, the DLVO potential is generally sufficient to describe the colloidal suspension behaviour. However, because of the van der Waals interactions, the DLVO potential $\rightarrow -\infty$ for surface-to-surface separation $h_{ij} \rightarrow 0$, which is not realistic. At very short distance, the interaction should intuitively be repulsive, because colloids cannot penetrate each other. In an aqueous medium, a repulsive hydration force ($U_{ij}^{\text{structural}}$) can be considered but in practice it is quite difficult to estimate it quantitatively from basic principles. For numerical purposes, this repulsive force is often modelled

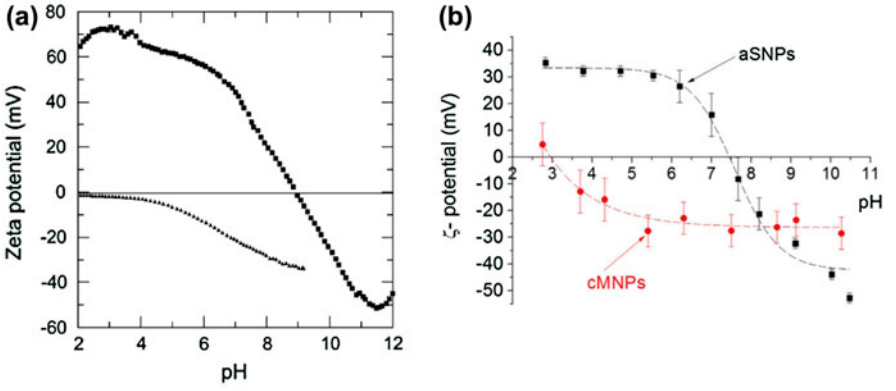

Figure 3. Zeta potential in two different binary colloidal systems as a function of pH.
Notes: (a) Alumina (squares) and silica (triangles) colloids. Reprinted with permission from Ref. [21]. Copyright 2008 American Chemical Society. (b) Carboxyl-functionalized silica-coated maghemite nanoparticles (cMNPs) and amino-functionalized silica nanoparticles (aSNPs). Reprinted with permission from Ref. [33]. Copyright 2015 Elsevier Science.

by phenomenological repulsion terms proportional to r^{-m}, where m is a positive exponent which is chosen to avoid significant superposition of colloids [48]. The resulting well depth at contact $-u_{\min}$ may be fitted to experimental data. For example, in [21,22], $u_{\min}$ was estimated by measuring the equilibrium adsorption of small silica colloids on the surface of large alumina colloids, a quantity which depends on the ratio $u_{\min}/(k_BT)$. The best agreement between the results given by the potential of Equation (1) and the measured adsorbed quantities was found for $14\,k_BT \leq u_{\min} \leq 16\,k_BT$ at room temperature. Superposition of colloids can be avoided also by imposing different types of constraint [49].

3. Aggregation processes, aggregate structures and gelification

Aggregate shapes in heteroaggregation can be quite different depending on several parameters, including the total volume fraction ϕ_s, the composition R of the suspension, the size difference between the two types of colloids, and all other parameters which define the colloid–colloid interactions.

Here we choose to consider separately two classes of heterogeneous systems, defined by the ratios between the average sizes of the components. As we will see, the aggregates in systems in which this ratio is very different from 1 are quite different from the aggregates formed by heterocolloids of equal size.

In the following the experimental results are compared to those of Brownian dynamics simulations [50]. In these simulations, the solvent is treated in an implicit way and its interaction with the colloids is given by a frictional force (proportional to the solvent viscosity) and a random force, usually called *noise*. These simulations allow to treat size and time scales comparable to those of several relevant experiments.

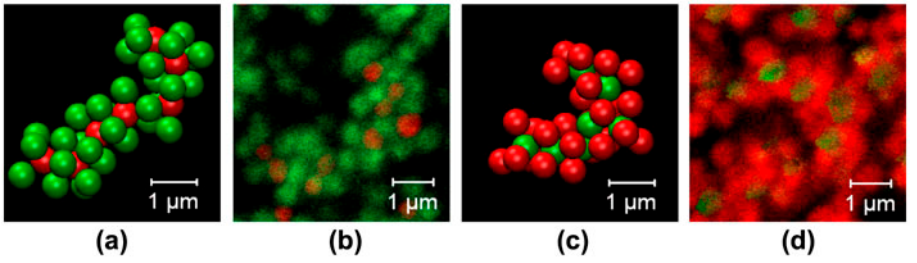

Figure 4. Internal structure of aggregates observed in suspensions with the majority of one type of particle: simulation snapshots for different mass ratios $R = m_{SiO_2}/(m_{Al_2O_3} + m_{SiO_2})$ (a) $R = 0.16$ and (c) $R = 0.82$ and confocal microscopy images for (b) $R = 0.16$ and (d) $R = 0.82$. Notes: Alumina and silica colloids have almost the same sizes (ratio between average diameters 1.06:1). Alumina and silica particles are green and red, respectively. Reprinted with permission from Ref. [26]. Copyright 2010 American Chemical Society.

3.1. Heterocolloids with moderate and small size mismatch

The heteroaggregation of colloids with moderate or small size mismatch has been extensively studied, with many efforts aiming at elucidating formation pathways and properties of colloidal crystals [2,3,6–8,29,51–59]. In the following we focus on the studies concerning ceramic colloids [16,17,23,24,26,28,31].

Cerbelaud et al. [23,24] and Piechowiak et al. [26,28] studied the heteroaggregation of alumina/silica colloids with size ratios 1.6:1 and 1.06:1, respectively. In the case of the almost equally sized colloids (with average radii a of about 300 nm), efforts were made to obtain spherical shapes for both types of particles. This was achieved by producing alumina-like particles, with a spherical silica core covered by a thin shell of alumina, in such a way that the surface chemistry of these particles was that of alumina. The particles were also functionalized by different dyes, so that alumina-like and silica particles appeared, respectively, green and red when imaged by a confocal microscope. The overall volume fraction of the colloids in the suspension was $\phi_s = 3\%$. In all cases, the experimental results were compared to those of Brownian dynamics simulations using the DLVO. Therefore $\kappa a \gg 1$, i.e. the Debye screening length was much smaller than the particle size. The simulations did not include gravity. However it has been shown that the effects of gravity are negligible for gel formation in binary colloids [7].

In both cases of 1.6:1 and 1:1 size ratios, the resulting aggregate shapes were non-compact and fractal like. Confocal microscopy images of typical aggregates obtained for 1:1 size ratio are shown in Figure 4, in which the experimental aggregates are compared to those obtained in the Brownian dynamics simulations. The agreement between experiments and simulations is striking, not only qualitatively but also quantitatively, as it follows from the analysis of the radial distribution functions of the colloids in the aggregates [26,28].

As can be seen in Figure 4, when the composition is strongly unbalanced between the two types of particles, the minority particles (silica in Figure 4(a) and (b) and alumina in 4(c) and (d)) constitute the backbone of the aggregates,

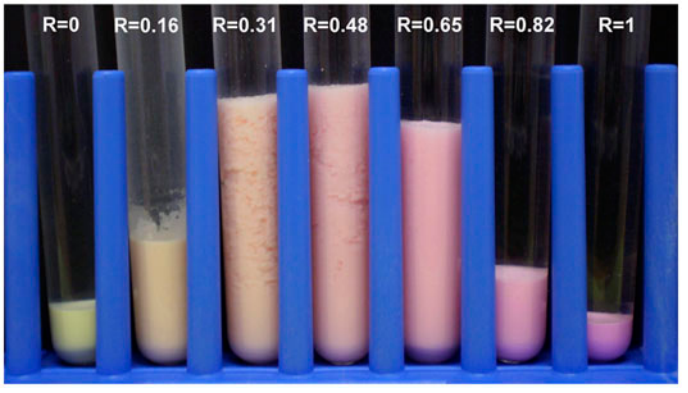

Figure 5. Images of sedimented suspensions of mixed- labelled alumina-like and silica particles as a function of different mass ratios $R = m_{SiO_2}/(m_{Al_2O_3} + m_{SiO_2})$ after 1 month. Note that the total volume fraction of colloids in the initial suspension is $\phi_s = 3\%$. This implies that most of the volume in the sediments at $R = 0.31$, 0.48 and 0.65 is indeed occupied by water, which is entrapped inside the network of colloids. Reprinted with permission from Ref. [26]. Copyright 2010 American Chemical Society.

Table 1. Colloid volume fractions ϕ_g in the sediments of Figure 5 as a function of $R = m_{SiO_2}/(m_{Al_2O_3} + m_{SiO_2})$. m_{SiO_2} and $m_{Al_2O_3}$ are the total masses of alumina and silica in the suspensions. ϕ_g is larger than the overall volume fraction $\phi_s = 3\%$ in the initial suspension because of the separation of the system between the precipitate and a part containing essentially pure solvent.

R	0.16	0.31	0.48	0.65	0.82
ϕ_g (%)	13.5	6.4	6.1	7.0	19.6

Note: Data taken from Ref. [26]. Copyright 2010 American Chemical Society.

while the majority particles surround the backbone, thus appearing on the aggregate surface. Aggregates of this type tend to repel each other, thus strongly hindering the formation not only of compact structures, but also of extended non-compact networks. Since relatively small aggregates are formed, sedimentation is quite slow for these unbalanced compositions. Extended networks are more easily formed for balanced compositions. These networks present a fractal character, in agreement with the results in [16,17].

The formation of extended fractal networks, which is achieved for reasonably balanced compositions (mass ratios $R = m_{SiO_2}/(m_{Al_2O_3} + m_{SiO_2}) = 0.31, 0.48$, 0.65) leads to fast precipitation giving gel-like cakes, as those shown in Figure 5. In these precipitates, most of the volume is indeed occupied by water. The observation of these precipitates allows further comparison between experiments and the simulations. In this comparison, the simulations are used to determine the colloid volume fraction at which a percolating network of colloids is formed. The comparison with the experiment is made by the following line of reasoning.

Let us assume that the powder volume fraction in the precipitates corresponds to the maximum density that can be achieved by the heteroaggregation process

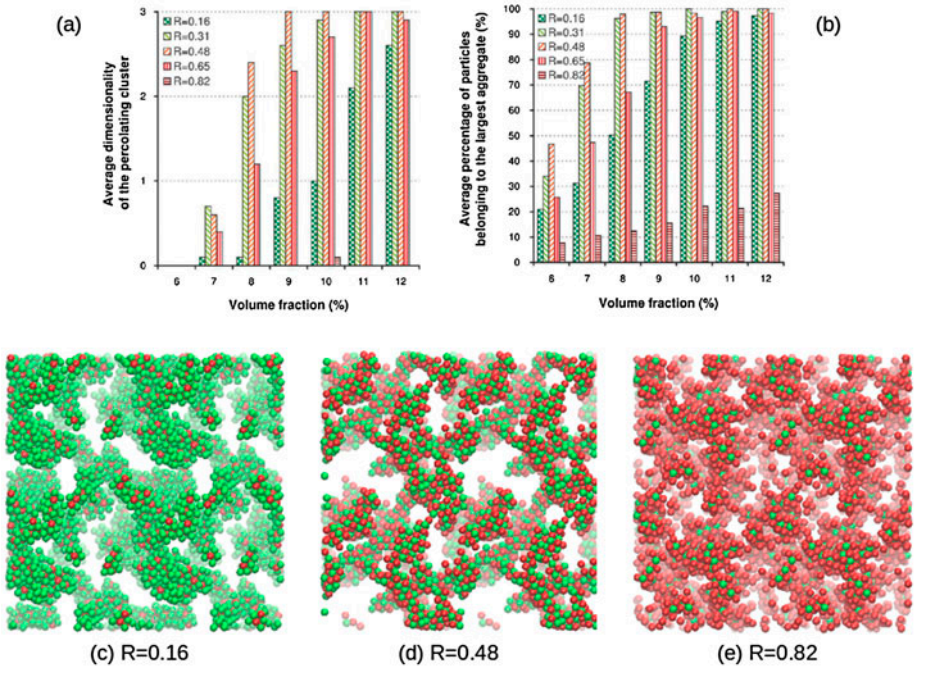

Figure 6. Brownian simulation results for the alumina–silica system with size ratio close to 1. Notes: (a) Percolation dimension. The percolation dimension counts the number of directions in which the largest aggregate spans the whole simulation box. (b) Number of colloids in the largest aggregate. Both quantities are given as functions of the overall volume fraction ϕ_s for different mass ratios R. (c), (d) and (e): snapshots of simulations at $\phi = 10\%$ and different R values. Only the snapshot in (d) shows a percolating aggregate. Reproduced with permission from Ref. [28] with permission from the PCCP Owner Societies.

at the corresponding composition. From this assumption, it follows that the sediment volume fraction corresponds to the density at which a percolating network is formed. Therefore, we can compare the experimental colloid volume fractions in the sediments to the volume fractions at which percolating networks start to form in the simulations. The sediment volume fractions are reported in Table 1. The results of the percolation simulations are shown in Figure 6.

The agreement between experiments and simulations is quite good: for $R = 0.31$, 0.48 and 0.65 the volume fractions ϕ_g in the sediments are between 6 and 7%, whereas in the simulations percolation appears for volume fractions between 7 and 8%. Moreover, in both experiments and simulations, percolation is easier for $R = 0.16$ than for $R = 0.82$. In fact, the simulations show that percolation occurs at volume fractions between 10 and 11% for $R = 0.16$, while percolation is not observed for $R = 0.82$ up to volume fractions of 12%.

Weston et al. [31] studied gel formation and shear thinning for binary mixtures of silica and alumina, silica and titania, and alumina and titania fumed nanoparticles in different solvents. Depending on solvent and on pH, Weston et al. found that pseudosolid gels at total colloid volume fractions ϕ_s as low as 1.5%

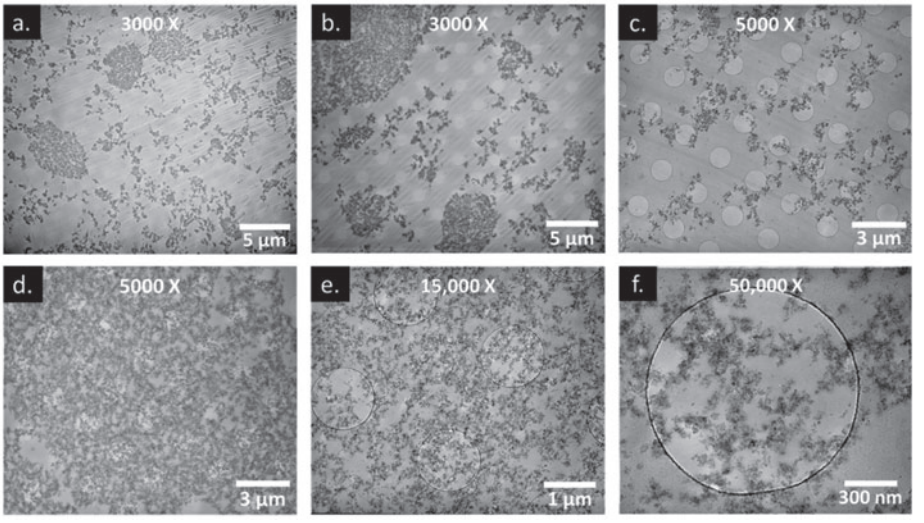

Figure 7. TEM micrographs illustrating areas of low particle density, containing dispersed nanoparticle aggregates of a variety of sizes with empty void spaces between them (ac), and a series of micrographs showing a region of unbroken nanoparticle networks that extend for tens of microns in all directions, at three different levels of magnification. Images are of ~100 nm thick sections of a 1.5 vol% 30-70 AluC-Aerosil 200 dispersions in polymerized LR white resin. Circles in background are from TEM grid.
Notes: Reprinted with permission from Ref. [31]. Copyright 2014 American Chemical Society.

can be formed. Representative results are shown in Figure 7. Fractal dimensions in the range of 2.3 were measured. Similar fractal dimensions were also obtained in suspensions with spherical colloids [16,17]. They are somewhat smaller than those predicted for diffusion-limited aggregation in three dimensions [60].

As in the case studied in [28], the formation of low-density gels was attributed to the competition between heterogeneous attractive interactions and homogeneous repulsive interactions hindering the rearrangement in the aggregates towards more compact shapes. This is indeed a result which is valid in general for binary colloids, besides ceramic systems. In fact, gel formation in binary colloids has been studied in several papers [7,8,55,56] about model systems such as polystyrene spheres. Specifically, in [56] it has been demonstrated that binary colloids tend to form less dense gels than unary colloids.

3.2. *Heterocolloids with large size mismatch*

The heteroaggregation of colloids with considerable size mismatch has been recently investigated in a series of papers, in which quite different systems were studied [9,10,14–22,27,33,55,61–63]. In the following we focus on results related to colloids used in ceramic processing.

Yates et al. [16] studied the heteroaggregation of alumina and silica colloids in a wide range of different size ratios, from about 70:1 to about 1:1. They noted that quite small mass ratios of small silica colloids, of the order of a few per cent,

are sufficient to induce the aggregation of larger, oppositely charged alumina colloids, a result that has been confirmed by subsequent works. In Ref. [17], the fractal dimension of the aggregates was measured at increasing silica/alumina size ratio, finding some increase, from 2.04 to 2.19, between the two extreme size ratios. This increase was attributed to the strengthening of the particle–particle interactions as the silica particle size grew larger.

Cerbelaud et al. [21] produced alumina/silica suspensions with huge size mismatch between the particles of average radii $a_{Al_2O_3} = 200$ and $a_{SiO_2} = 12.5$ nm, giving a size ratio of 16:1. The pH range was between 6.5 and 8, in which these colloids acquire opposite charges (see Figure 3(a)). The large, positively charged, alumina colloids presented quite irregular shapes, while the small negative silica colloids were spherical to a very good degree of approximation. In these experiments the amount of silica particles adsorbed on the alumina ones was at first determined, using inductively coupled plasma (ICP) analysis [19]. As shown in Figure 8, with increasing silica content, the adsorption measurements became incompatible both with the hypothesis of full adsorption and with the hypothesis of adsorption limited by charge neutralization. For 3% total mass fraction R of added silica ($R = m_{SiO_2}/(m_{Al_2O_3} + m_{SiO_2})$), the amount of silica adsorbed on alumina was significantly smaller than the total amount of silica, but significantly larger than the amount needed to neutralize the positive charge of alumina. The Brownian simulations using the DLVO potential were able to reproduce quantitatively the experimental behaviour. The value of the inverse Debye length was $\kappa = 10^8$ m^{-1}, so that $\kappa a_{Al_2O_3} \gg 1$ and $\kappa a_{SiO_2} \simeq 1$.

The shapes of the resulting aggregates were then imaged by scanning electron microscopy (Cryo-FEGSEM), revealing a typical aggregation pattern which was also qualitatively reproduced by the Brownian dynamics simulations. In this pattern, several small silica colloids form a ring in between two neighbour alumina particles, as shown in Figure 9(a) and (b). The silica colloids in the ring are co-adsorbed between two alumina particles. The silica rings thus compensate for the electrostatic repulsion between adjacent alumina particles, in such a way that aggregates can form. Because of ring formation, the amount of silica needed to induce aggregation was quite small, since aggregation was observed for mass fractions of 0.2 and 1.1%, that are much smaller than the amount needed to neutralize the overall alumina particle charge by adsorption. The formation of a ring can be considered as a form of bridging aggregation [64], a phenomenon which is induced in most cases using co-adsorbed polymers as bridging agents.

The Brownian simulations revealed that the aggregation process consists of two steps [22]

(a) A fast initial stage, which is completed on a time scale of 10^{-2}-10^{-1} s, in which the silica colloids adsorb on isolated alumina particles and reach the stationary coverage.

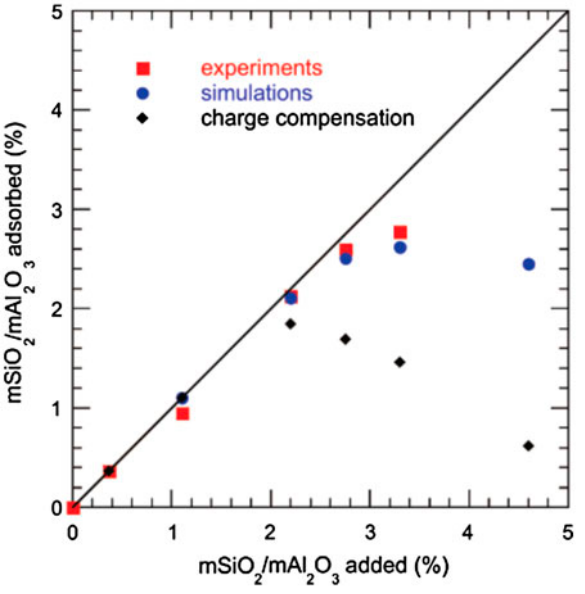

Figure 8. Comparison between the adsorption isotherm of silica on an alumina surface measured experimentally by ICP analysis (■), the one calculated from the simulation results (•), and the simple scaling estimates of adsorption based on charge compensation (◆). The straight line indicates complete adsorption.
Notes: Reprinted with permission from Ref. [21]. Copyright 2008 American Chemical Society.

(b) A subsequent slower agglomeration process, in which the silica-covered alumina particles diffuse, meet and begin to form aggregates.

Step (b) was fast if the concentration of silica nanoparticles was not too large [22]. In fact, for relatively high silica concentrations (mass fraction $R = 3.3\%$) a large number of silica particles covered each alumina particle forming a rather rigid network on it. The overall charge of the silica-covered alumina particles was negative (see the charge compensation model in Figure 8). Even though aggregation was shown to be energetically favourable, it required rearrangement of the silica particle network, a process that was unlikely to take place on the scale of 0.1 s reached by the simulations. However, the experiments, performed on much longer time scales, did show aggregation also for $R = 3.3\%$.

This is at variance with some of the results by Gilchrist et al. [15], who determined the structural evolution of colloidal phases assembled from oppositely charged mixtures of silica microspheres and polystyrene nanoparticles, with size ratio 60:1. Individual suspensions of either type of particle were stable, but heteroflocculation took place upon mixing them, depending on the number ratio of small to large species. At low nanoparticle concentrations, nanoparticle bridges form between microspheres, leading to their flocculation, while at higher concentrations the nanoparticles form a denser coating on the microsphere surfaces, inducing charge reversal and, ultimately, their restabilization.

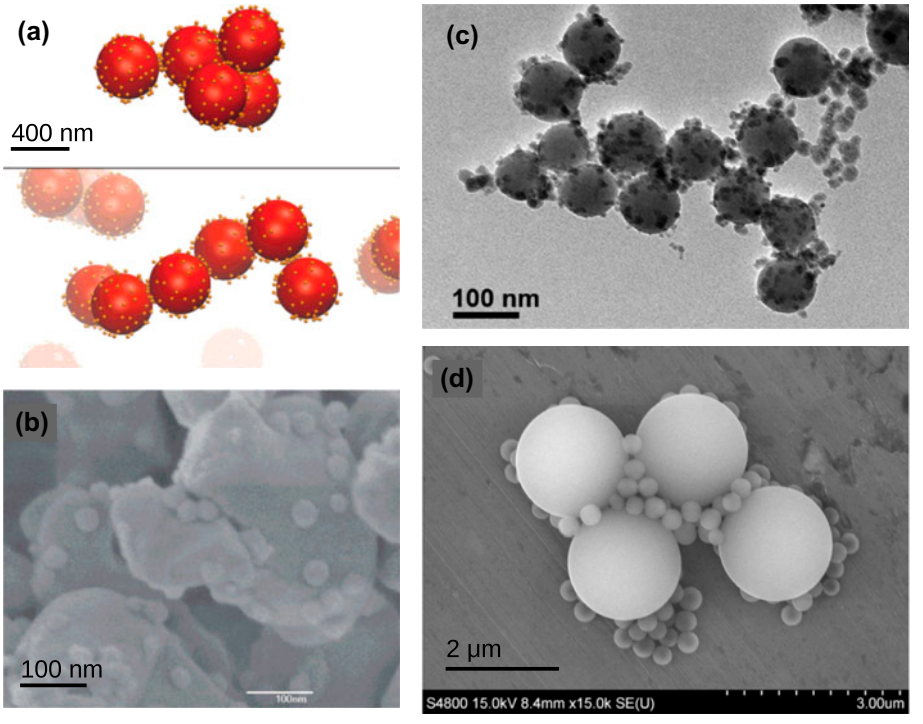

Figure 9. Images of heteroaggregates of colloids with huge size difference, showing the formation of a ring of small colloids between the large ones. (a) and (b) Brownian-simulation and experimental cryo-FEGSEM images of aggregates of large alumina and small silica colloids (ratio between average sizes 16:1). The experimental alumina colloids have irregular shapes, while silica colloids are spherical. In (a), the horizontal line separates two different simulation snapshots. Reprinted with permission from Ref. [21]. Copyright 2008 American Chemical Society. (c) TEM image of carboxyl-functionalized silica-coated maghemite nanoparticles (cMNPs) and amino-functionalized silica nanoparticles (aSNPs), with size ratio 3.8:1. Reprinted with permission from Ref. [33]. Copyright 2015 Elsevier Science. (d) SEM image of a heteroaggregate consisting of 4 polystyrene particles and several melamine–formaldehyde particles, with size ratio 5.46:1. Reprinted with permission from Ref. [10]. Copyright 2009 Elsevier Science.

Concerning the aggregate shapes, both experiments and simulations [21,22] showed that it is possible to obtain both chain-like and compact alumina–silica aggregates in this system with huge size mismatch. Compact aggregates are energetically favourable, so that chain-like aggregates have a tendency to rearrange thus becoming compact. However kinetic factors may hinder this process.

Dusak et al. [33] studied the aggregation of carboxyl-functionalized silica-coated maghemite nanoparticles (cMNPs) and amino-functionalized silica nanoparticles (aSNPs), with size ratio 3.8:1. As shown in Figure 3(b), aSNPs and cMNPs were positively and negatively charged, respectively. The resulting aggregates showed again the emergence of the typical aggregation pattern (Figure 9(c)) in which small particles form rings that are able to bridge between large particles. The experimental evidence for these rings was even more evident than in [21], because in [33] both types of particles were essentially spherical.

Suspensions of TiO_2 nanoparticles with smectite clays have been studied by Labille et al. [65], showing that nanoparticle behaviour is mainly driven by heteroaggregation with clay colloids (due to electrostatic forces), while homoaggregation remains negligible. Primary heteroaggregates were formed via the attachment of nanoparticles to the clay. This was followed by a secondary heteroaggregation stage by bridging nanoparticles.

Since the driving force towards the formation of these types of aggregates is of quite general character, we expect to find them in other colloidal systems besides ceramic colloids, such as latex spheres [9,10,63]. This is indeed the case, as can be seen for example in Figure 9(d), in which aggregates of polystyrene particles and melamine–formaldehyde particles with size ratio 5.46:1 are shown. Aggregation with formation of rings of small colloids bridging larger ones has been also observed in [63], where suspensions of polystyrene latex (size ∼530 nm) and alumina-coated silica (primary ∼12 nm) colloids have been studied and their rheological properties have been determined.

These results show that the main driving force for aggregation, i.e. electrostatic attraction between unlike colloids, leads to the formation of quite similar aggregate morphologies in quite different systems.

There are systems in which the aggregation mechanism by ring formation is not observed. As example of this is the silica–zirconia system which has been experimentally studied in [14] and simulated in [18]. In that system, silica colloids are larger than zirconia colloids by a factor 10^2. Silica colloids are assumed to have zero potential, while zirconia colloids are strongly charged and induce local opposite charge when they adsorb on silica. The resulting attraction is extremely short-ranged compared to the size of the silica colloids, since its range is estimated to be about 1/600 of the silica colloid size. These facts render co-adsorption of zirconia on silica extremely unlikely, so that the rings cannot form. In alumina–silica, the attraction range [21] is about 1/40 of the alumina size.

4. Discussion and conclusions

In most of the heteroaggregation phenomena treated in Section 3, the heteroaggregation of ceramic colloids is mostly driven by screened electrostatic interactions (of inverse screening length κ) when the colloids are sufficiently far apart. Because of electrostatics, unlike colloids tend to approach each other, while like colloids are forced to stay separated. When unlike colloids come into contact, also other forces, including van der Waals attraction and structural force, come into play, giving rise to a potential well of finite depth $-u_{\min}$.

Let us discuss first the case in which the two types of colloids have similar radii of magnitude a. In this case, the most important parameters determining heteroaggregation are $u_{\min}/(k_BT)$ and κa. Typical values of κ for ceramic colloids are in the range of 10^8 m^{-1} [21,26], which, for submicron colloids, gives $\kappa a \gg 1$. This interaction range is very short compared to the size of the colloids, so that in

an aggregate, a colloid strongly interacts only with its nearest neighbours, which are colloids of the other type. Colloid–colloid electrostatic attraction is thus of the *sticky* type [66]. Some weak attractive interaction with the colloids of the same type may be caused by the shallow secondary minimum due the van der Waals contribution. Typical values of $u_{\min}$ can well exceed $10\,k_BT$, as in the alumina–silica system at room temperature [21,22]. Both the sticky character and the deep well of the interactions contribute to cause a difficult rearrangement of colloids in the aggregates. The results of this difficult rearrangement is the formation of thin, fractal-like aggregates, which is at the origin of the low percolation thresholds encountered in several cases [16,17,28,31].

An easier rearrangement of the colloids would lead to more compact shapes. This can be achieved in principle by decreasing κa and $u_{\min}/k_BT$. The effect of decreasing $u_{\min}$ has been confirmed by a series of Brownian dynamics simulations [28,58]. κa can be decreased using nanocolloids, i.e. colloids with radii in the range of a few 10 nm, and/or by changing the solvent properties to achieve significantly larger κ. Decreasing $u_{\min}/(k_BT)$ implies controlling the interaction of colloids when they come into contact. This may be achieved by properly functionalizing the colloid surfaces. If the aim is to produce not only compact aggregates but true colloidal crystals, size dispersion must be very narrow and colloid shapes very regular. Moreover, secondary-minimum effects may be tuned in such a way that they match the periodicity of the crystal.

For colloids with large size mismatch (say of radii a_1 and a_2, with $a_1 \gg a_2$), one may have $\kappa a_1 \gg 1$ but $\kappa a_2 \simeq 1$. In this case, small colloids can rather easily rearrange when adsorbed on the large colloids. A common aggregation pattern, in which small colloids bridge between large colloids forming rings or necks between them, is observed in a variety of ceramic and other systems [9,10,21,22,33,63]. In this case, not only chain-like aggregates, but also compact ones can be formed.

The different compactness of the aggregates formed in suspension can have consequences on the subsequent steps of ceramic processing. An important issue in this case is to produce uniform materials with controlled porosity. As we have seen, for alumina–silica, the aggregates were more compact in a system with large size mismatch (16:1) than in a system with small size mismatch (1.6:1) [24]. After aggregation, both systems were used to form millimetric spheres by a granulation process [19,20]. At the end of the granulation process, the spheres presented outer homogeneous size and shape in both cases, but their internal structures were different. For 16:1 size ratio, the porosity in the spheres was homogeneously distributed, except for the appearance of some cracks. For 1.6:1 size ratio, spheres exhibited a central large cavity free of solid. This difference was attributed to the intra-aggregate porosity. After being produced in the liquid, the spheres were dried and sintered. Capillary forces during drying may bring the particles from the sphere centre to its surface. Thus, one may expect that the

more porous the aggregate is in the liquid, the larger the cavity inside the spheres will be at the end.

Disclosure statement

No potential conflict of interest was reported by the authors.

References

[1] J.A. Lewis, J. Am. Cer. Soc. 83 (2000) p.2341.
[2] J.M. López-López, A. Schmitt, A. Moncho-Jordá and R. Hidalgo-Álvarez, Soft Matter 2 (2006) p.1025.
[3] J.M. López-López, A. Schmitt, A. Moncho-Jordá and R. Hidalgo-Álvarez, Adv. Colloid Interface Sci. 147–148 (2009) p.186.
[4] A.F. Demirörs, J.C.P. Stiefelhagen, T. Vissers, F. Smallenburg, M. Dijkstra, A. Imhof and A. van Blaaderen, Phys. Rev. X 5 (2015) p.021012.
[5] W. Lin, M. Kobayashi, M. Skarba, C. Mu, P. Galletto and M. Borkovec, Langmuir 22 (2006) p.1038.
[6] M.E. Leunissen, C.G. Christova, A.P. Hynninen, C.P. Royall, A.I. Campbell, A. Imhof, M. Dijkstra, R. van Roij and A. van Blaaderen, Nature 437 (2005) p.235.
[7] E. Sanz, M.E. Leunissen, A. Fortini, A. van Blaaderen and M. Dijkstra, J. Phys. Chem. B 112 (2008) p.10861.
[8] E. Sanz, C. Valeriani, T. Vissers, A. Fortini, M.E. Leunissen, A. van Blaaderen, D. Frenkel and M. Dijkstra, J. Phys.: Condens. Matter 20 (2008) p.494247.
[9] S. Rollie and K. Sundmacher, Langmuir 24 (2008) p.13348.
[10] S. Rollié, H. Briesen and K. Sundmacher, J. Colloid Interface Sci. 336 (2009) p.551.
[11] Y. Mao and D.J. McClements, Food Hydrocolloids 25 (2011) p.1201–1209.
[12] Y. Mao and D.J. McClements, Food Hydrocolloids 27 (2012) p.80.
[13] Y. Mao and D.J. McClements, J. Appl. Polym. Sci. 130 (2013) p.3833.
[14] V. Tohver, J.E. Smay, A. Braem, P.V. Braun and J.A. Lewis, Proc. Natl. Acad. Sci. USA 98 (2001) p.8950.
[15] J.F. Gilchrist, A.T. Chan, E.R. Weeks and J.A. Lewis, Langmuir 21 (2005) p.11040.
[16] P.D. Yates, G.V. Franks, S. Biggs and G.J. Jameson, Colloids Surf. A 255 (2005) p.85.
[17] P.D. Yates, G.V. Franks and G.J. Jameson, Colloids Surf. A 326 (2008) p.83.
[18] J. Liu and E. Luijten, Phys. Rev. E 72 (2005) p.061401.
[19] P. Garcia-Perez, C. Pagnoux, F. Rossignol and J.-F. Baumard, Colloids Surf. A 281 (2006) p.58.
[20] P. Garcia-Perez, C. Pagnoux, A. Pringuet, A. Videcoq and J.-F. Baumard, J. Colloid Interface Sci. 313 (2007) p.527.
[21] M. Cerbelaud, A. Videcoq, P. Abélard, C. Pagnoux, F. Rossignol and R. Ferrando, Langmuir 24 (2008) p.3001.
[22] M. Cerbelaud, A. Videcoq, P. Abélard and R. Ferrando, J. Colloid Interface Sci. 332 (2009) p.360.
[23] M. Cerbelaud, R. Ferrando and A. Videcoq, J. Chem. Phys. 132 (2010) p.084701.
[24] M. Cerbelaud, A. Videcoq, P. Abélard, C. Pagnoux, F. Rossignol and R. Ferrando, Soft Matter 6 (2010) p.370.
[25] S. Perko, A. Dakskobler and T. Kosmac, J. Am. Ceram. Soc. 93 (2010) p.2499.
[26] M.A. Piechowiak, A. Videcoq, F. Rossignol, C. Pagnoux, C. Carrion, M. Cerbelaud and R. Ferrando, Langmuir 26 (2010) p.12540.

[27] S. Barg, B.P. Binks, H. Wang, D. Koch and G. Grathwohl, J. Porous Mater. 19 (2012) p.859.
[28] M.A. Piechowiak, A. Videcoq, R. Ferrando, D. Bochicchio, C. Pagnoux and F. Rossignol, Phys. Chem. Chem. Phys. 14 (2012) p.1431.
[29] N. Siedl, S.O. Baumann, M.J. Elser and O. Diwald, J. Phys. Chem. C 116 (2012) p.22967.
[30] V.M. Candelario, M.I. Nieto, F. Guiberteau, R. Moreno and A.L. Ortiz, J. Eur. Ceram. Soc. 33 (2013) p.1685.
[31] J.S. Weston, D. Venkataramani, C.P. Aichele, B.P. Grady, J. Harwell and D. Resasco, Langmuir 30 (2014) p.14982.
[32] Y. Fan, M. Estili, G. Igarashi, W. Jiang and A. Kawasaki, J. Eur. Ceram. Soc. 34 (2014) p.443.
[33] P. Dušak, A. Mertelj, S. Kralj and D. Markovec, J. Colloid Interface Sci. 438 (2015) p.235.
[34] G. Trefalt, B. Tadfic and M. Kosec, Soft Matter 7 (2011) p.5566.
[35] J. Lyklema, *Fundamentals of Interface and Colloid Science*, Vol. 1, Academic Press, London, 1991.
[36] N.I. Lebovka, Adv. Polym. Sci. 255 (2014) p.57.
[37] N. Jacob, *Israelachvili, editor. Intermolecular and Surface Forces (Second Edition)*, 3rd ed., Academic Press, San Diego, 1991.
[38] Y. Liang, N. Hilal, P. Langston and V. Starov, Adv. Colloid Interface Sci. 134–135 (2007) p.151.
[39] B.V. Derjaguin and L. Landau, Acta Physicochim. URSS 14 (1941) p.633.
[40] E.J.W. Verwey and J.Th.G. Overbeek, *Theory of the Stability of Lyophobic Colloids*, Elsevier, Amsterdam, 1948.
[41] G. Trefalt, S.H. Behrens and M. Borkovec, Langmuir 32 (2015) p.380.
[42] M. Elimelech, J. Gregory, X. Jia and R.A. Williams, *Particle Deposition and Aggregation: Measurement, Modelling and Simulation*, Butterworth-Heinemann, Oxford, 1995.
[43] R. Hogg, T.W. Healy and D.W. Fuerstenau, Trans. Faraday Soc. 62 (1966) p.1638.
[44] T.W. Healy, G.R. Wiese, D.E. Yates and B.V. Kavanagh, J. Colloid Interface Sci. 42 (1973) p.647.
[45] E.J.W. Verwey and J.T.G. Overbeek, *Theory of the Stability of Lyophobic Colloids*, Dover Publications, Mineola, New York, 1999.
[46] A.V. Delgado, F. Gonzáles-Caballero, R.J. Hunter, L.K. Koopal and J. Lyklema, J. Colloid Interface Sci. 309 (2007) p.194.
[47] F.J.M. Ruiz-Cabello, P. Maroni and M. Borkovec, J. Chem. Phys. 138 (2013) p.234705.
[48] M. Hecht, J. Harting, T. Ihle and H.J. Herrmann, Phys. Rev. E. 72 (2005) p.011408.
[49] M. Hütter, J. Colloid Interface Sci. 231 (2000) p.337.
[50] M.P. Allen and D.J. Tildesley, *Computer Simulation of Liquids*, Oxford University Press, Oxford, 1987.
[51] P. Bartlett and A.I. Campbell, Phys. Rev. Lett. 95 (2005) p.128302.
[52] A.-P. Hynninen, M.E. Leunissen, A. van Blaaderen and M. Dijkstra, Phys. Rev. Lett. 96 (2006) p.018303.
[53] M. Bier, R. van Roij and M. Dijkstra, J. Chem. Phys. 133 (2010) p.124501.
[54] E. Dickinson, J. Colloid Interface Sci. 356 (2011) p.196.
[55] E. Spruijt, H.E. Bakker, T.E. Kodger, J. Sprakel and M.A. Cohen Stuart, Soft Matter 7 (2011) p.8281.
[56] E.R. Russell, J. Sprakel, T.E. Kodger and D.A. Weitz, Soft Matter 8 (2012) p.8697.
[57] G. Pavaskar, S. Sharma and S.N. Punnathanam, J. Chem. Phys. 136 (2012) p.134506.
[58] D. Bochicchio, A. Videcoq and R. Ferrando, Phys. Rev. E 87 (2013) p.022304.
[59] D. Bochicchio, A. Videcoq and R. Ferrando, J. Chem. Phys. 140 (2014) p.024911.
[60] S. Tolman and P. Meakin, Physica A 158 (1989) p.801.

[61] C. Pagnoux, N. Tessier-Doyen, A. Pringuet, M. Cerbelaud and P. Garcia-Perez, J. Eur. Ceram. Soc. 29 (2009) p.1379.
[62] K. Prabhakaran, R. Sooraj, C.S. Kumbhar, A. Melkeri, N.M. Gokhale and S.C. Sharma, Ceram. Int. 36 (2010) p.1.
[63] J. Lee, S.J. Lee, K.H. Ahn and S.J. Lee, Langmuir 31 (2015) p.16639.
[64] S. Biggs, M. Habgood, G.J. Jameson and Y.-D. Yan, Chem. Eng. J. 80 (2000) p.13.
[65] J. Labille, C. Harns and J.-Y. Bottero, J. Brant. Environ. Sci. Technol. 49 (2015) p.6608.
[66] J.P.K. Doye, D.J. Wales and R.S. Berry, J. Chem. Phys. 103 (1995) p.4234.